LIMNOLOGY
and
OCEANOGRAPHY

ASLO

Limnol. Oceanogr. 60, 2015, 1619–1633

doi: 10.1002/lno.10124

Dissolved silicon isotopic compositions in the East China Sea: Water mass mixing vs. biological fractionation

Zhimian Cao,*[1] Martin Frank,[1] Minhan Dai[2]

[1]GEOMAR Helmholtz Center for Ocean Research Kiel, Kiel, Schleswig-Holstein, Germany

[2]State Key Laboratory of Marine Environmental Science, Xiamen University, Xiang'an District, Xiamen, Fujian, China

Abstract

We present the first set of dissolved silicon isotope data in seawater ($\delta^{30}Si_{Si(OH)4}$) from the East China Sea, a large and productive marginal sea significantly influenced by the Kuroshio Current and freshwater inputs from the Changjiang (Yangtze River). In summer (August 2009), the lowest surface $\delta^{30}Si_{Si(OH)4}$ signatures of +2.1‰ corresponding to the highest $Si(OH)_4$ concentrations (~30.0 μmol L^{-1}) were observed nearshore in Changjiang Diluted Water. During advection on the East China Sea inner shelf, surface $\delta^{30}Si_{Si(OH)4}$ increased rapidly to +3.2‰ while $Si(OH)_4$ became depleted, indicating increasing biological utilization of the $Si(OH)_4$ originating from the Changjiang Diluted Water. This is also reflected in the water column profiles characterized by a general decrease of $\delta^{30}Si_{Si(OH)4}$ and an increase of $Si(OH)_4$ with depth on the East China Sea mid-shelf and slope. In winter (December 2009–January 2010), however, the $\delta^{30}Si_{Si(OH)4}$ was nearly constant at +1.9‰ throughout the water column on the East China Sea shelf beyond the nearshore, which was a consequence of enhanced vertical mixing of the Kuroshio subsurface water. Horizontal admixture of Kuroshio surface water, which is highly fractionated in Si isotopes, was observed only beyond the shelf break. Significant seasonal differences in $\delta^{30}Si_{Si(OH)4}$ were detected in the surface waters beyond the Changjiang Diluted Water-influenced region on the East China Sea shelf, where the winter values were ~1.0‰ lower than those in summer, despite the same primary $Si(OH)_4$ supply from the Kuroshio subsurface water during both seasons. This demonstrates significantly higher biological consumption and utilization of $Si(OH)_4$ in summer than in winter.

The stable silicon isotopic composition of dissolved silicic acid ($\delta^{30}Si_{Si(OH)4}$) is a sensitive tracer of the biogeochemical cycling of Si in both the open ocean (e.g., Reynolds et al. 2006; de Souza et al. 2012; Grasse et al. 2013) and marginal seas (Cao et al. 2012; Ehlert et al. 2012). The main processes controlling seawater $\delta^{30}Si_{Si(OH)4}$ signatures are $Si(OH)_4$ utilization by diatoms, biogenic silica (BSi) dissolution, and water mass mixing. While previous studies revealed that diatoms preferentially incorporate lighter Si isotopes from surrounding seawater with a relatively constant fractionation factor ($^{30}\varepsilon_{upt}$) of −1.1‰ (De La Rocha et al. 1997; Fripiat et al. 2011, and references therein), new culture experiments showed that the $^{30}\varepsilon_{upt}$ of polar/subpolar diatom species varies within a relatively large range of −0.5 to −2.1‰ (Sutton et al. 2013). On the other hand, based on experiments Demarest et al. (2009) suggested that the lighter Si isotopes are preferentially released into seawater during BSi dissolution with a fractionation factor ($^{30}\varepsilon_{diss}$) of −0.55‰, whereas near zero values of $^{30}\varepsilon_{diss}$ were observed in laboratory dissolution experiments using, respectively, an estuarine diatom species (−0.12‰; Sun et al. 2014) and diatom opal extracted from sediments (+0.14‰; Wetzel et al. 2014). Although no fractionation occurs during water mass mixing, this physical process primarily determines the initial $Si(OH)_4$ concentration and its isotopic composition for diatom growth, which are not spatially and/or temporally homogenous in a given oceanic system (Cardinal et al. 2005; Fripiat et al. 2011), in particular in marginal seas with highly dynamic hydrographic conditions (Cao et al. 2012).

The East China Sea is the largest temperate marginal sea of the western North Pacific, with an area of ~0.7×10^6 km^2 and an average depth of ~300 m (Wong et al. 2000). It is characterized by a broad shelf significantly fed by the world's fourth largest river, the Changjiang (Yangtze River), and a direct link with the western North Pacific through the western boundary current, the Kuroshio Current. Rich supplies of nutrients from the upwelling of Kuroshio subsurface water (Chen 1996) as well as the Changjiang discharge (Li et al.

*Corresponding author: zcao@geomar.de

2007) stimulate high primary production (PP) on the East China Sea shelf resulting in one of the most productive areas of the world's oceans (Liu et al. 2010). Moreover, the East China Sea is characterized by a distinct seasonal pattern of warm summers (22.0-28.0°C) and colder winters (9.0-21.0°C) (Han et al. 2013). PP in winter is approximately one order of magnitude lower than the 200-1000 mg C m^{-2} d^{-1} reached in summer, primarily due to poor growth conditions such as reduced light availability (Gong et al. 2003; Chiang et al. 2004; Liu et al. 2010).

As a result of the overall eutrophic condition on the East China Sea shelf, the phytoplankton abundance is frequently dominated by diatoms, which, however, show large spatial and seasonal variations (Furuya et al. 1996; Chiang et al. 1999; Furuya et al. 2003; Chiang et al. 2004; Guo et al. 2014). In later spring/summer, the highest abundances of diatoms (exceeding 10^5 cells L^{-1}) are observed on the inner shelf associated with the Changjiang plume, whereas the abundance decreases rapidly toward the mid-shelf and the shelf edge to levels of $<10^4$ cells L^{-1} (Chiang et al. 1999; Furuya et al. 2003). In contrast, the absolute abundance of diatoms in winter is significantly lower within a range of 10^3 to 10^4 cells L^{-1}. While the lowest winter diatom abundances (below 10^3 cells L^{-1}) are observed along the Chinese coastline in the southern East China Sea, elevated amounts of diatoms with abundances $>10^4$ cells L^{-1} are occasionally distributed along the surface of the East China Sea shelf break (Chiang et al. 2004).

Moreover, human activities including dam construction and coastal eutrophication are exerting high influence on the East China Sea river-coast ecosystem. It has been documented that the building of the Three Gorges Dam has resulted in a significant decrease of the $Si(OH)_4$ loading to the East China Sea (Gong et al. 2006), while the increased application of fertilizers has increased riverine inputs of dissolved nitrogen (N) and phosphorus (Li et al. 2007). As a consequence, a sharp drop in $Si(OH)_4$ to nitrate (NO_3) ratio (Gong et al. 2006) now limits diatom growth in river-influenced regions of the East China Sea, where the phytoplankton species shift from siliceous algae to nonsiliceous algae has induced frequent harmful algal blooms in nearshore waters (Li et al. 2007).

In this context, diatoms play variable roles in different areas and seasons of the East China Sea associated with complex physicobiogeochemical conditions and even anthropogenic pressure. With the goal to identify the different $Si(OH)_4$ sources for diatom growth and to examine $Si(OH)_4$ utilization and/or regeneration during BSi production/dissolution, we analyzed the horizontal and vertical distribution of dissolved Si isotopic composition of seawater in summer and winter 2009. Our data demonstrate highly variable $Si(OH)_4$ supply to different areas of the East China Sea and significant biological fractionation of Si isotopes in summer compared with minor $Si(OH)_4$ utilization in winter. In addition, the in situ fractionation factor $^{30}\varepsilon_{upt}$ in the East China Sea is evaluated via identifying the initial conditions followed by point-by-point calculations with field $\delta^{30}Si_{Si(OH)4}$ data, and is compared to previous results.

Materials and methods

Study area

The East China Sea extends from Cheju Island in the north to the northern coast of Taiwan in the south, and is bounded by the Okinawa Trough in the east and the coast of China in the west. Nearly 70% of the sea lies on the continental shelf with the shelf break located at about 170 m (Fig. 1; Wong et al. 2000). Shelf circulation in the East China Sea is driven by the East Asian Monsoon with the strong northeast monsoon prevailing from September to April and the relatively weak southwest monsoon from May to August (Liu et al. 2003). The Kuroshio Current flows northeastward along the East China Sea continental slope, while the Kuroshio Branch Current separates from the main Kuroshio Current path and flows onto the shelf in a westward direction. The Kuroshio Branch Current west of Kyushu forms the origin of the Tsushima Strait Warm Current flowing into the Japan Sea and the Yellow Sea Warm Current flowing into the Yellow Sea (Fig. 1; Ichikawa and Beardsley 2002). Additional features include the southward flowing China Coastal Current during winter and the northward expansion of the Taiwan Warm Current from the Taiwan Strait in summer (Fig. 1; Lee and Chao 2003). Amongst the various rivers in eastern China flowing into the East China Sea, the Changjiang is the largest with a peak water discharge of 50,000 m^3 s^{-1} in summer and a minimum of 13,000 m^3 s^{-1} in winter (http://xxfb.hydroinfo.gov.cn/). The pathway of the Changjiang Diluted Water is largely controlled by the shelf circulation pattern resulting in dispersion towards the north and east in summer but southward flow as part of the China Coastal Current along the Chinese coast in winter (Fig.1; Lee and Chao 2003).

Sampling and analysis

Sampling was conducted onboard the R/V *Dongfanghong* II during a summer (18-29 August 2009; Wang et al. 2014) and a winter (23 December 2009– 5 January 2010) cruise. Seawater samples for $\delta^{30}Si_{Si(OH)4}$ and $Si(OH)_4$ concentration analyses were collected at stations PN10, PN08, PN06, and PN04, plus DH13 in summer and PN03b in winter extending from near the mouth of the Changjiang estuary to the continental slope area (Fig. 1). 100−250 mL of seawater was collected with Niskin bottles attached to a Rosette sampler and filtered through 0.45 μm nitrocellulose acetate filters into acid precleaned polyethylene bottles. $\delta^{30}Si_{Si(OH)4}$ samples were subsequently acidified to pH∼2 with distilled concentrated HCl (0.1% v/v) and stored at room temperature in the dark, while $Si(OH)_4$ concentrations were analyzed onboard immediately. At stations PN08 and PN04, suspended particle

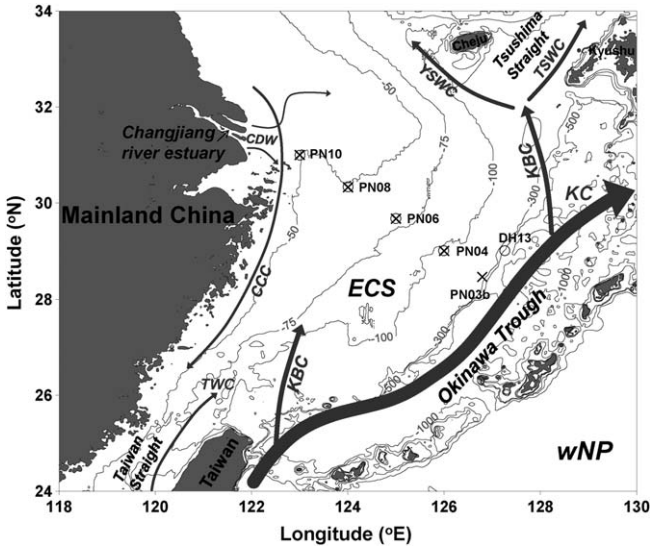

Fig. 1. Map of the East China Sea (ECS) including bathymetry and the locations of sampling stations in summer (circles) and winter (crosses) 2009. Schematically shown is the surface circulation pattern according to Ichikawa and Beardsley (2002, and references therein). KC: Kuroshio Current; KBC: Kuroshio Branch Current; TSWC: Tsushima Strait Warm Current; YSWC: Yellow Sea Warm Current; TWC: Taiwan Warm Current; CCC: China Coastal Current; CDW: Changjiang Diluted Water. wNP: the western North Pacific.

samples for BSi analyses were obtained on both cruises by filtering ~2 L of seawater through 0.4 μm polycarbonate membranes. The membranes were dried at 50°C overnight and stored in polycarbonate dishes for analysis in the home laboratory.

The dissolved $Si(OH)_4$ in the seawater samples for isotope analyses was separated from the major matrix elements using a two-step brucite-coprecipitation technique adapted from the MAGIC method (Karl and Tien 1992). Samples with $Si(OH)_4$ concentrations lower than 10 μmol L^{-1} were preconcentrated through repeated precipitation applying the same two-step technique (Ehlert et al. 2012; Grasse et al. 2013). After removing the supernatant of 40 mL of each seawater sample, the first brucite precipitates were redissolved in small amounts of 6 M HCl and an extra 10 mL of the sample was added. The precipitation procedure was repeated by twice adding 1% v/v of 1 M NaOH. Through repeated precipitation, the low $Si(OH)_4$ content in the surface water samples was preconcentrated by at least a factor of 30 to a concentration of ~65 μmol L^{-1}, while the magnesium content in the final solutions for column chemistry was at the same time significantly reduced. For deep waters with high $Si(OH)_4$ concentrations above 10 μmol L^{-1}, only 5 mL of seawater and one precipitation step were required for analysis. All precipitates were redissolved in small amounts of 6 M HCl. Given that nearly 100% of the dissolved $Si(OH)_4$ was removed from the seawater samples by this coprecipitation method, it can be assumed that no significant fractionation affecting the final $\delta^{30}Si_{Si(OH)4}$ results occurred (Cardinal et al. 2005; Reynolds et al. 2006).

The Si in the resulting solutions was further purified using a cation-exchange chromatography procedure adapted from Georg et al. (2006). Si isotopic compositions were determined on a Nu Plasma HR MC-ICPMS at GEOMAR, Kiel, equipped with an adjustable source-defining slit set at pseudo high-resolution mode for separation of the ^{30}Si beam from molecular interference. For each sample 2 mL of solution with a Si concentration of ~20 μmol L^{-1} was measured three to five times following a standard-sample-standard bracketing technique. All solutions were introduced into a dry plasma achieved using a Cetac Aridus II desolvator equipped with a PFA nebulizer with an uptake rate of 60 μL min^{-1}.

$\delta^{30}Si$ values are reported in ‰ deviations from the international Si standard NBS28 ($\delta^{30}Si = [(^{30}Si/^{28}Si)_{sample}/(^{30}Si/^{28}Si)_{NBS28} - 1] \times 1000$). External reproducibility is given as 2 standard deviations (2SD) of the average $\delta^{30}Si$ value from either the bracketing measurements of the same sample solution during a single day ($2SD_{bracketing}$) or repeated sample measurements on different days ($2SD_{repeated}$), which represents the error bars of field $\delta^{30}Si_{Si(OH)4}$ data provided in this contribution (Figs. 3-5). The $2SD_{bracketing}$ of all samples in this study varied between ±0.05 and ±0.35‰, which were comparable to $2SD_{repeated}$ of selected samples within a range of ±0.00 to ±0.36‰ (Table 1). Repeated measurements of the standard reference materials IRMM-018 and Big Batch gave average $\delta^{30}Si$ values of -1.55 ± 0.19‰ (2SD, $n = 46$) and -10.62 ± 0.25‰ (2SD, $n = 43$), which agree well with the values obtained during an interlaboratory comparison experiment (Reynolds et al. 2007). The long-term external reproducibility for the replicate measurements of an in-house seawater matrix standard was ±0.25‰ (2SD, $n = 18$).

Vertical profiles of temperature and salinity were determined shipboard with a calibrated SBE-19-plus Conductivity-Temperature-Depth recorder (Sea-Bird Co.) attached to the Rosette sampler. $Si(OH)_4$ concentration data were obtained onboard using a Technicon AA3 Auto-Analyzer (Bran-Luebbe, GmbH Co.) following classical colorimetric methods, which had a precision of ±3% (1SD; Du et al. 2013). BSi concentrations were also measured on the Technicon AA3 Auto-Analyzer after a two-step wet-alkaline digestion following Ragueneau et al. (2005). Repeated measurements gave an uncertainty of the entire procedure of <±10% (1SD; Liu et al. 2011).

Modeling Si isotope fractionation during $Si(OH)_4$ utilization

Si isotope fractionation during $Si(OH)_4$ utilization by diatoms can be described using either a Rayleigh or a steady state model (Cao et al. 2012, and references therein). The

Table 1. Salinity, silicic acid ($Si(OH)_4$) concentration and their stable silicon isotopic composition ($\delta^{30}Si_{Si(OH)4}$) data collected during summer and winter cruises to the East China Sea (ECS) in August 2009 and December 2009–January 2010.

					Bracketing measurements						Repeated measurements	
					I		II		III			
					$\delta^{30}Si_{Si(OH)4}$		$\delta^{30}Si_{Si(OH)4}$		$\delta^{30}Si_{Si(OH)4}$		$\delta^{30}Si_{Si(OH)4}$	
Cruise	Station	Depth (m)	Salinity	$Si(OH)_4$ ($\mu mol\ L^{-1}$)	(‰ ± $2SD_{bracketing}$‡)	n*	(‰ ± $2SD_{bracketing}$‡)	n*	(‰ ± $2SD_{bracketing}$‡)	n*	(‰ ± $2SD_{repeated}$§)	N†
ECS	PN10	1.3	25.89	27.93	2.18 ± 0.31	5	2.24 ± 0.30	3			2.21 ± 0.09	2
summer	31.0°N	4.5	27.17	30.16	1.93 ± 0.26	5						
2009	123.0°E	14.9	32.22	27.22	1.95 ± 0.25	4	1.70 ± 0.25	4			1.83 ± 0.35	2
		25.1	34.00	25.97								
		35.5	34.11	25.95								
		46.9	34.13	25.94	1.65 ± 0.25	4	1.51 ± 0.24	4			1.58 ± 0.20	2
	PN08	1.7	31.84	0.89	3.15 ± 0.21	5	3.28 ± 0.34	3			3.21 ± 0.18	2
	30.3°N	5.4	31.87	1.33	3.19 ± 0.16	4						
	124.0°E	14.7	33.53	3.18	2.62 ± 0.22	5						
		25.0	33.80	6.39	2.22 ± 0.25	5	2.26 ± 0.32	3	1.98 ± 0.14	4	2.15 ± 0.31	3
		34.4	33.82	15.15								
		48.6	33.82	21.22	2.04 ± 0.26	5						
	PN06	1.9	33.45	2.06	2.78 ± 0.31	4	3.04 ± 0.33	4	2.89 ± 0.21	3	2.90 ± 0.26	3
	29.7°N	14.6	33.57	2.23								
	125.0°E	24.5	33.59	2.15	2.48 ± 0.29	5	2.39 ± 0.20	4			2.44 ± 0.12	2
		34.3	33.76	4.64	2.20 ± 0.28	4	2.35 ± 0.28	3	1.99 ± 0.20	4	2.18 ± 0.36	3
		50.4	34.19	12.37								
		81.1	34.22	12.75	2.01 ± 0.21	5						
	PN04	2.0	33.74	1.95	2.76 ± 0.33	5	3.01 ± 0.23	4	2.84 ± 0.16	3	2.87 ± 0.26	3
	29.0°N	14.7	33.75	1.98								
	126.0°E	24.4	33.83	1.85	2.99 ± 0.34	4						
		49.4	33.85	1.91								
		73.8	34.10	5.39	2.12 ± 0.24	3	2.24 ± 0.21	5			2.18 ± 0.17	2
		99.8	34.50	11.46								
		117.7	34.50	11.50	2.12 ± 0.23	5	1.98 ± 0.21	4	2.05 ± 0.24	3	2.05 ± 0.14	3
	DH13	3.2	33.73	0.99	3.00 ± 0.22	5	2.95 ± 0.28	4			2.97 ± 0.07	2
	29.0°N	25.1	33.82	1.00	2.85 ± 0.27							
	127.3°E	73.8	34.18	1.17	2.77 ± 0.24	3	2.54 ± 0.34	3	2.52 ± 0.28	5	2.61 ± 0.28	3
		98.6	34.39	3.04								
		123.7	34.61	6.59	1.74 ± 0.24	5	1.97 ± 0.25	4			1.86 ± 0.33	2
		148.6	34.49	13.17								
		198.5	34.45	24.51	1.62 ± 0.28	4						
		297.3	34.37	34.59								
		553.7	34.33	69.06	1.69 ± 0.32	4	1.68 ± 0.08	4			1.69 ± 0.03	2
ECS	PN10	2.7	33.74	9.22	2.45 ± 0.33	5	2.47 ± 0.21	4			2.46 ± 0.04	2
winter	31.0°N	25.0	33.74	8.70	2.49 ± 0.26	4	2.29 ± 0.25	3			2.39 ± 0.29	2
2009	123.0°E	48.2	33.74	8.70	2.50 ± 0.28	5						
	PN08	1.2	33.99	6.00	2.00 ± 0.28	4	2.09 ± 0.35	3			2.05 ± 0.14	2
	30.3°N	24.6	33.99	6.00								
	124.0°E	46.6	33.98	5.99	2.20 ± 0.25	5	2.25 ± 0.21	3			2.22 ± 0.08	2
	PN06	1.7	34.03	7.12	1.90 ± 0.33	4	1.90 ± 0.30	3			1.90 ± 0.00	2
	29.7°N	26.5	34.03	7.12	1.85 ± 0.27	3						
	125.0°E	80.5	34.03	7.12	1.89 ± 0.31	5	1.99 ± 0.17	4			1.94 ± 0.14	2

TABLE 1. Continued

					Bracketing measurements						Repeated measurements	
					I		II		III			
					$\delta^{30}Si_{Si(OH)4}$		$\delta^{30}Si_{Si(OH)4}$		$\delta^{30}Si_{Si(OH)4}$		$\delta^{30}Si_{Si(OH)4}$	
Cruise	Station	Depth (m)	Salinity	$Si(OH)_4$ ($\mu mol\ L^{-1}$)	(‰ ± $2SD_{bracketing}$‡)	n*	(‰± $2SD_{bracketing}$‡)	n*	(‰± $2SD_{bracketing}$‡)	n*	(‰± $2SD_{repeated}$§)	N†
	PN04	2.9	34.34	5.67	1.90 ± 0.31	5	1.99 ± 0.31	4			1.95 ± 0.12	2
	29.0°N	24.6	34.34	5.66								
	126.0°E	49.4	34.33	5.64	1.84 ± 0.21	5	1.99 ± 0.25	3			1.91 ± 0.21	2
		74.9	34.33	5.62								
		100.0	34.33	5.51								
		116.1	34.34	5.49	1.69 ± 0.27	3	1.84 ± 0.31	3	1.64 ± 0.28	5	1.72 ± 0.22	3
	PN03b	4.1	34.62	1.00	2.73 ± 0.20	3	2.76 ± 0.33	4			2.74 ± 0.03	2
	28.5°N	50.6	34.61	1.00	2.76 ± 0.21	3						
	126.8°E	73.8	34.54	1.05	2.58 ± 0.32	4	2.56 ± 0.31	4			2.57 ± 0.02	2
		102.6	34.54	1.23	2.25 ± 0.23	5	2.45 ± 0.13	3			2.35 ± 0.28	2
		152.3	34.61	7.28	1.59 ± 0.13	5	1.47 ± 0.05	4			1.53 ± 0.16	2
		201.4	34.45	23.09	1.44 ± 0.33	5	1.26 ± 0.16	4			1.35 ± 0.24	2

*n is the number of bracketing measurements for the $\delta^{30}Si$ of a single sample solution in a single day.
†N is the number of repeated sample measurements for the $\delta^{30}Si$ on different days.
‡‰ ± $2SD_{bracketing}$ is the average $\delta^{30}Si$ together with 2 standard deviations estimated from the bracketing measurements in a single day.
§‰ ± $2SD_{repeated}$ is the average $\delta^{30}Si$ together with 2 standard deviations estimated from the repeated sample measurements on different days.

Rayleigh model assumes a system with no further supply of $Si(OH)_4$ from external sources, and is illustrated by the following equations:

$$\delta^{30}Si_{Si(OH)4_{observed}} = \delta^{30}Si_{Si(OH)4_{initial}} + {}^{30}\varepsilon_{upt} \times \ln f \quad (1)$$

$$f = \frac{[Si(OH)_4]_{observed}}{[Si(OH)_4]_{initial}} \quad (2)$$

The subscript "observed" and "initial" denote measured $\delta^{30}Si_{Si(OH)4}$ and $Si(OH)_4$ values at any given time and those prior to biological utilization, respectively. The term f indicates the fraction of remaining dissolved $Si(OH)_4$ in solution relative to the initial concentration. The fractionation factor ${}^{30}\varepsilon_{upt}$ is thus estimated as:

$${}^{30}\varepsilon_{upt} = \frac{\delta^{30}Si_{Si(OH)4_{observed}} - \delta^{30}Si_{Si(OH)4_{initial}}}{\ln f} = \frac{\delta^{30}Si_{Si(OH)4_{observed}} - \delta^{30}Si_{Si(OH)4_{initial}}}{\ln \frac{[Si(OH)_4]_{observed}}{[Si(OH)_4]_{initial}}} \quad (3)$$

Alternatively, the steady state model describes the evolution of $\delta^{30}Si_{Si(OH)4}$ assuming a system with a continuous supply of $Si(OH)_4$ with a given isotopic composition:

$$\delta^{30}Si_{Si(OH)4_{observed}} = \delta^{30}Si_{Si(OH)4_{initial}} - {}^{30}\varepsilon_{upt} \times (1-f) \quad (4)$$

In this case ${}^{30}\varepsilon_{upt}$ is calculated as:

$${}^{30}\varepsilon_{upt} = \frac{\delta^{30}Si_{Si(OH)4_{initial}} - \delta^{30}Si_{Si(OH)4_{observed}}}{1-f} = \frac{\delta^{30}Si_{Si(OH)4_{initial}} - \delta^{30}Si_{Si(OH)4_{observed}}}{1 - \frac{[Si(OH)_4]_{observed}}{[Si(OH)_4]_{initial}}} \quad (5)$$

In both models, $\delta^{30}Si_{Si(OH)4observed}$ and $[Si(OH)_4]_{observed}$ represent the field data measured in this study. The validation of initial values, i.e., the $Si(OH)_4$ sources for diatom growth, is of importance for the precise estimation of ${}^{30}\varepsilon_{upt}$ in different areas of the East China Sea.

Results

Hydrography

As demonstrated by the temperature-salinity (T-S) diagrams, stations PN10, PN08, PN06, and PN04 on the East China Sea shelf were strongly stratified in summer, displaying increasing salinity and decreasing potential temperature (PT) with increasing density (σ_0) levels (Fig. 2a). In winter, however, the entire water column at these stations was thoroughly mixed as demonstrated by uniform PT and salinity values (Fig. 2b).

On the inner shelf, the summer surface waters (top 7 m, $\sigma_0 < 19.0$) at the innermost station PN10 featured Changjiang Diluted Water with PT > 24.0°C and salinity <29.0 (Fig. 2a). The salinity of the surface waters ($\sigma_0 \sim 19.5$) at the following station PN08 remained low at <32.0 while PT was >29.0°C reflecting weakened influence of the Changjiang Diluted

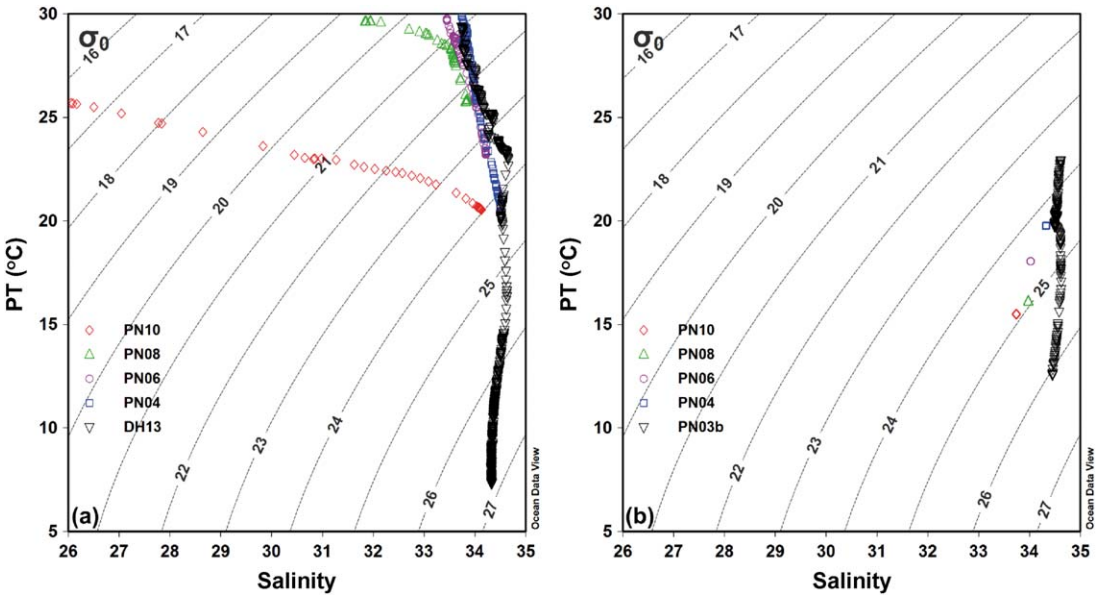

Fig. 2. Potential temperature (PT) vs. salinity plots (T-S diagram) for the sampling stations in (a) summer and (b) winter 2009. The gray lines indicate the isopycnals (σ_0). Note that PT and salinity values at stations PN10, PN08, PN06, and PN04 in winter were essentially constant throughout the water column. The plots were created with ODV (Schlitzer, 2015). [Color figure can be viewed in the online issue, which is available at wileyonlinelibrary.com.]

Water. T-S distribution patterns at stations PN06 and PN04 on the mid-shelf in summer were comparable to those of the upper 100 m of the water column (σ_0 <23.5) at station DH13 beyond the shelf edge (Fig. 2a). Its surface water salinity was higher than on the inner shelf, but still lower than 34.0 reflecting typical shelf water without significant intrusion of more saline Kuroshio Branch Current waters (Chern et al. 1990; Chen et al. 1995). A salinity maximum of >34.6 was observed in the subsurface waters around 120-160 m (σ_0 ~23.5-25.3) at station DH13 (Fig. 2a), which marks admixture of the Kuroshio Tropical Water sourced in the subtropical North Pacific (Chen et al. 1995; Suga et al. 2000).

In winter, surface PTs of 15.5-23.0°C were significantly lower than in summer, while salinity varied within a much smaller range of 33.7 to 34.6 (Fig. 2b). The overall higher salinity indicates that waters in the sampling area were dominated by the Kuroshio Branch Current extending towards the shelf, with even negligible dilution of the surface waters at the innermost station PN10 by the fresh China Coastal Current. At station PN03b near the shelf break, the subsurface salinity maximum around 150 m (σ_0 ~25.0) was not clearly distinguishable owing to the comparable surface salinities above 34.6 (Fig. 2b).

Spatial and seasonal distributions of $Si(OH)_4$ and $\delta^{30}Si_{Si(OH)4}$

Due to the large input of nutrients from the Changjiang in summer, surface $Si(OH)_4$ concentrations reached their highest values of ~30.0 μmol L^{-1} at station PN10, which is comparable to the subsurface waters below (Fig. 3f). Surface $\delta^{30}Si_{Si(OH)4}$ values around +2.1‰ were within analytical error identical to or slightly higher than those in the deep waters (Fig. 3k; Table 1). However, the summer surface $Si(OH)_4$ at the other four stations was highly depleted (Fig. 3g–j) corresponding to heavy $\delta^{30}Si_{Si(OH)4}$ signatures of ~+3.0‰ (Fig. 3l–o; Table 1). At stations PN08, PN06 and PN04 on the East China Sea shelf (Fig. 3b–d), $Si(OH)_4$ generally increased (Fig. 3g–i) and $\delta^{30}Si_{Si(OH)4}$ decreased with water depth. $\delta^{30}Si_{Si(OH)4}$ values around +2.0‰ in the near-bottom waters were ~1.0‰ lower than the surface waters (Fig. 3l–n; Table 1). At station DH13, located in the slope area, extremely low $Si(OH)_4$ concentrations of 1.0 μmol L^{-1} were observed above 75 m in summer, which below increased markedly from the 75 m depth to the bottom (Fig. 3j). The $\delta^{30}Si_{Si(OH)4}$ signatures display an overall inverse trend decreasing rapidly from the surface to 125 m depth and remaining essentially stable at +1.6‰ below (Fig. 3o; Table 1).

In winter, salinity (Fig. 3a–d), $Si(OH)_4$ (Fig. 3f–i) and $\delta^{30}Si_{Si(OH)4}$ signatures (Fig. 3k–n) were nearly constant throughout the water column at stations PN10, PN08, PN06, and PN04 on the East China Sea shelf but the $\delta^{30}Si_{Si(OH)4}$ signatures at station PN10 were slightly heavier than those of the other three stations (+2.5 vs. +1.9‰; Table 1). At station PN03b located beyond the East China Sea shelf edge, $Si(OH)_4$ was depleted above 100 m water depth and then increased rapidly below (Fig. 3j). Correspondingly, $\delta^{30}Si_{Si(OH)4}$ decreased slightly from the surface (+2.8‰) to 100 m depth (+2.3‰) followed by a sharp decrease to the bottom (+1.4‰; Fig. 3o; Table 1).

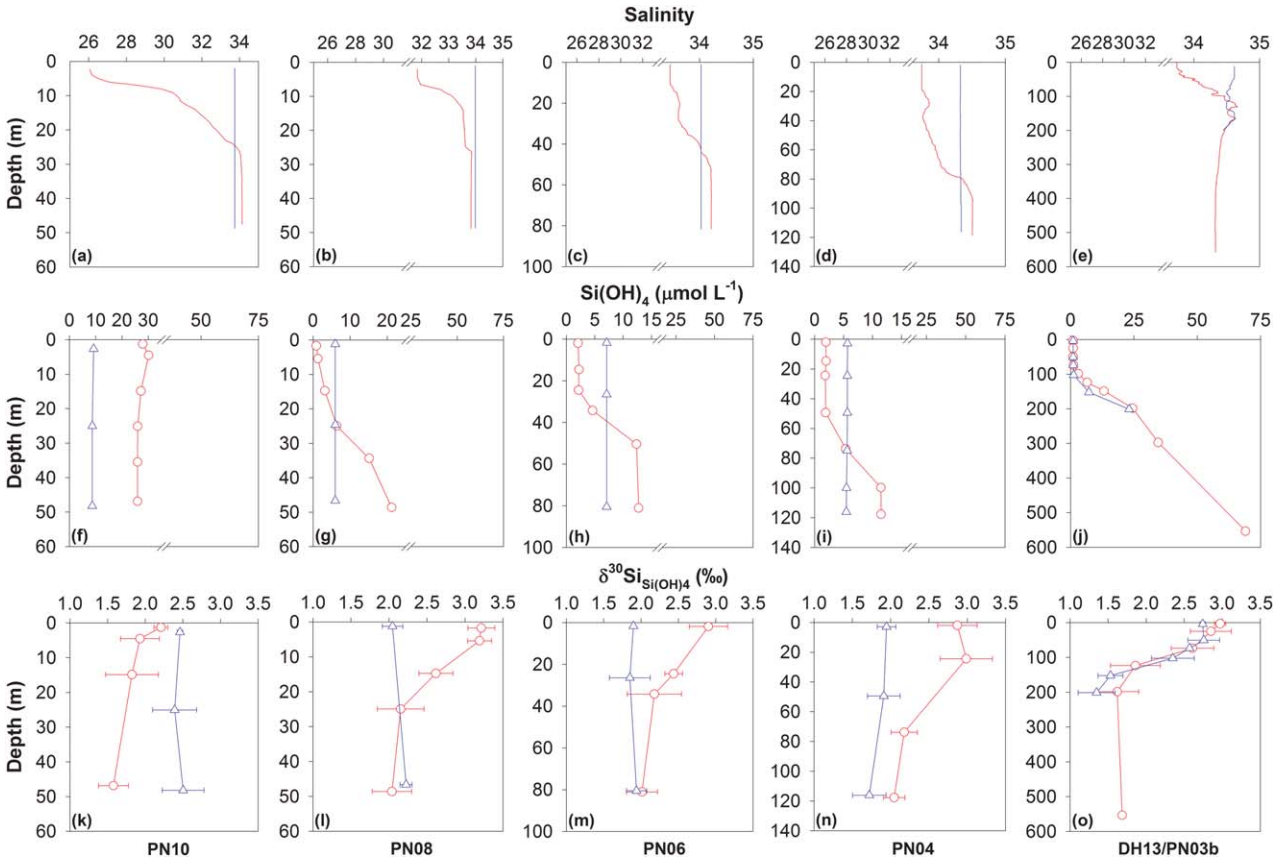

Fig. 3. Vertical distribution of (top) salinity, (middle) $Si(OH)_4$ and (bottom) $\delta^{30}Si_{Si(OH)4}$ at the sampling stations in summer (red circles and lines) and winter (blue triangles and lines) 2009. (a) PN10: Salinity; (b) PN08: Salinity; (c) PN06: Salinity; (d) PN04: Salinity; (e) DH13/PN03b: Salinity; (f) PN10: $Si(OH)_4$; (g) PN08: $Si(OH)_4$; (h) PN06: $Si(OH)_4$; (i) PN04: $Si(OH)_4$; (j) DH13/PN03b: $Si(OH)_4$; (k) PN10: $\delta^{30}Si_{Si(OH)4}$; (l) PN08: $\delta^{30}Si_{Si(OH)4}$; (m) PN06: $\delta^{30}Si_{Si(OH)4}$; (n) PN04: $\delta^{30}Si_{Si(OH)4}$; (o) DH13/PN03b: $\delta^{30}Si_{Si(OH)4}$. [Color figure can be viewed in the online issue, which is available at wileyonlinelibrary.com.]

$Si(OH)_4$ concentrations at station PN10 were overall three times higher in summer than in winter and coincided with lighter summer $\delta^{30}Si_{Si(OH)4}$ signatures throughout the water column, in particular in the near-bottom waters where the summer value of +1.6‰ was significantly lower than +2.5‰ in winter (Fig. 3k; Table 1). In contrast, distinct $\delta^{30}Si_{Si(OH)4}$ differences between summer and winter were only detected in the surface waters at stations PN08, PN06, and PN04, in that the winter values of ~+2.0‰ accompanied by higher winter $Si(OH)_4$ concentrations (Fig. 3g–i) were lower than those near +3.0‰ in summer (Fig. 3l-n; Table 1). No significant $\delta^{30}Si_{Si(OH)4}$ differences outside analytical error were observed between stations DH13 and PN03b (Fig. 3o) despite the fact that the subsurface $Si(OH)_4$ concentrations around 100-200 m were overall lower in winter than in summer (e.g., 7.3 vs. 13.2 μmol L^{-1} at 150 m depth; Fig. 3j; Table 1). At the subsurface salinity maximum a $\delta^{30}Si_{Si(OH)4}$ value of +1.5 ± 0.2‰ near the 150 m depth at station PN03b in winter was slightly lower but analytically indistinguishable from that of +1.9 ± 0.3‰ at 125 m depth at station DH13 in summer (Fig. 3o; Table 1).

Discussion

Dynamics of dissolved Si isotopes in the East China Sea in summer

Biological fractionation during horizontal admixture of the Changjiang Diluted Water

The T-S data show that in summer the Changjiang Diluted Water dominated the surface layer of the innermost station PN10 at a salinity of ~26.0 while its influence was already strongly reduced at station PN08 on the East China Sea inner shelf as suggested by a salinity of ~32.0 (Fig. 2a). The outermost station DH13 was characterized by a surface salinity close to 34.0 (Fig. 2a) reflecting the East China Sea surface water end-member of the cross shelf mixing with the Changjiang Diluted Water, which is in agreement with previous hydrographic studies on the eastward extension of Changjiang Diluted Water (e.g., Lie et al. 2003; Chen et al. 2008). Moreover, a highly significant linear relationship between total alkalinity (considered as a (quasi)conservative chemical tracer) and salinity was observed in the surface waters along our section from the nearshore to the slope

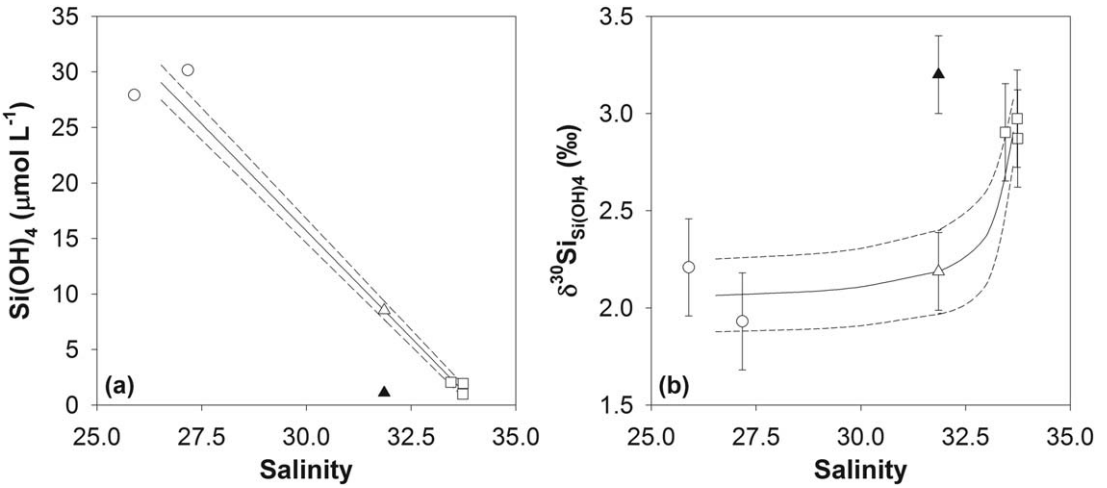

Fig. 4. (a) $Si(OH)_4$ and (b) $\delta^{30}Si_{Si(OH)4}$ vs. salinity during the mixing between the Changjiang Diluted Water and the East China Sea surface water in summer 2009. The solid lines represent the mixing curve between the two end-member waters. The dashed lines above and below indicate errors deduced from the uncertainties in estimating the end-member values, which are the standard deviation of field observations involved in the Changjiang Diluted Water (circles) and the East China Sea surface water (squares). The open triangles denote initial values of $Si(OH)_4$ and $\delta^{30}Si_{Si(OH)4}$ for the summer surface waters at station PN08 based on the conservative mixing, whereas the solid triangles denote the corresponding average values measured in the field. The distinct differences between them document fractionation of Si isotopes during biological utilization of dissolved $Si(OH)_4$.

area ($r^2 = 0.96$; data not shown) clearly supporting cross shelf mixing.

Correspondingly, the highest summer surface $Si(OH)_4$ concentration of 30.0 μmol L^{-1} was observed in the Changjiang Diluted Water at station PN10 and was already significantly depleted at the surface of station PN08 (Fig. 3f,g; Table 1). This marked decrease thus largely resulted from mixing with and dilution of surrounding $Si(OH)_4$-poor waters combined with the potentially enhanced utilization by diatoms during advection of the Changjiang Diluted Water, given that the high nutrient discharge within the river plume and the low turbidity of its lower reach are favorable for phytoplankton growth (Gaston et al. 2006, and references therein). In this context, the significantly higher surface $\delta^{30}Si_{Si(OH)4}$ values at station PN08 relative to those at station PN10 (+3.2 vs. +2.1‰; Fig. 3k,i; Table 1) were induced by biological fractionation of the $Si(OH)_4$ originating from the Changjiang Diluted Water.

Salinity, $Si(OH)_4$ concentration and $\delta^{30}Si_{Si(OH)4}$ values for the Changjiang Diluted Water end-member (i.e., the top 5 m waters at station PN10) were determined to be 26.5, 29.0 μmol L^{-1} and $+2.1 \pm 0.2$‰ (1SD, $n = 2$), respectively, which represent the averages of values collected from 2 and 5 m depths at station PN10. In contrast, salinity, $Si(OH)_4$ concentration and $\delta^{30}Si_{Si(OH)4}$ values for the East China Sea surface water end-member were estimated to be 33.6, 1.7 μmol L^{-1} and $+2.9 \pm 0.2$‰ (1SD, $n = 3$), respectively, which are the averages of values collected from 2 m depth at stations PN06, PN04, and DH13 in summer (Fig. 4). Simple mixing between the two end-members leading to an average salinity of 31.86 for the summer surface waters at station PN08 predicts a $Si(OH)_4$ concentration of 8.5 μmol L^{-1} (Fig. 4a) and a $\delta^{30}Si_{Si(OH)4}$ of $+2.2 \pm 0.2$‰ (Fig. 4b), which served as the initial condition for diatom growth in these waters (Table 2). The subsequent $Si(OH)_4$ utilization resulting in values as low as 1.1 μmol L^{-1} generated heavier $\delta^{30}Si_{Si(OH)4}$ signatures reaching an average value of $+3.2 \pm 0.2$‰ (1SD, $n = 2$; Fig. 4b).

The corresponding $^{30}\varepsilon_{upt}$ was estimated to be -0.5 ± 0.1‰ following the Rayleigh model (Eq. 3) and -1.1 ± 0.3‰ following the steady state model (Eq. 5) with an average f value of 0.13 (Eq. 2; Table 2). While both values are within the range obtained by Sutton et al. (2013), the latter is indistinguishable from the value of −1.1‰ obtained during the early culture experiments (De La Rocha et al. 1997). This consistence clearly suggests that our estimation of the initial condition based on cross shelf mixing was realistic. The difference in the $^{30}\varepsilon_{upt}$ values between the two models may have simply reflected that any natural system lies between an ideal Rayleigh one and an ideal steady state one, even though for our sampling sites the continuous Changjiang input of $Si(OH)_4$ in summer stimulating diatom growth in the surface waters on the East China Sea inner shelf within a steady state system is clearly more realistic.

Biological fractionation controlled by vertical supply of $Si(OH)_4$

At stations PN06, PN04, and DH13 beyond the Changjiang Diluted Water-influenced region, the summer vertical profiles of $\delta^{30}Si_{Si(OH)4}$ displayed a pattern generally observed in the world's oceans, which is characterized by an increase of $Si(OH)_4$ concentrations with increasing water depth (Fig.

Table 2. Estimations of the fractionation factor during diatom growth ($^{30}\varepsilon_{upt}$) in the East China Sea.

Season	Station	Depth (m)	$Si(OH)_4$ ($\mu mol\ L^{-1}$)	$\delta^{30}Si_{Si(OH)4}$ (‰)	f*	$^{30}\varepsilon_{upt}$ (‰ ± 1SD†) Rayleigh	$^{30}\varepsilon_{upt}$ (‰ ± 1SD†) Steady state
Summer	PN08	1.7	0.89	3.21	0.10	−0.45 ± 0.12	−1.15 ± 0.25
		5.4	1.33	3.19	0.16	−0.54 ± 0.14	−1.19 ± 0.28
Initial condition			*8.55*	*2.19*			
average						*−0.50 ± 0.13*	*−1.17 ± 0.26*
Summer	PN06	1.9	2.06	2.90	0.31	−0.90 ± 0.23	−1.52 ± 0.38
		24.5	2.15	2.44	0.33	−0.52 ± 0.23	−0.86 ± 0.38
	PN04	2.0	1.95	2.87	0.30	−0.83 ± 0.22	−1.44 ± 0.37
		24.4	1.85	2.99	0.28	−0.89 ± 0.21	−1.57 ± 0.36
	DH13	3.2	0.99	2.97	0.15	−0.59 ± 0.14	−1.31 ± 0.30
		25.1	1.00	2.85	0.15	−0.53 ± 0.14	−1.17 ± 0.30
Initial condition			*6.59*	*1.86*			
average						*−0.71 ± 0.20*	*−1.31 ± 0.35*
Winter	PN08	1.2	6.00	2.05	0.82	N.D‡	N.D
		46.6	5.99	2.22	0.82	N.D	N.D
	PN06	1.7	7.12	1.90	0.98	N.D	N.D
		26.5	7.12	1.85	0.98	N.D	N.D
		80.5	7.12	1.94	0.98	N.D	N.D
	PN04	2.9	5.67	1.95	0.78	N.D	N.D
		49.4	5.64	1.91	0.77	N.D	N.D
		116.1	5.49	1.72	0.75	N.D	N.D
Initial condition			*7.28*	*1.53*			
average						*N.D*	*N.D*

*f is the fraction of the $Si(OH)_4$ measured in the field relative to the initial $Si(OH)_4$ (Eq. 2).
†‰ ± 1SD is the average $^{30}\varepsilon_{upt}$ together with 1 standard deviation estimated from the uncertainties of the initial values, which are analytical errors of ±0.25‰ for $\delta^{30}Si_{Si(OH)4}$ determination and of ±3% for $Si(OH)_4$ concentration determination.
‡N.D denotes "not determined" as the negligible biological utilization would result in large uncertainties when estimating $^{30}\varepsilon_{upt}$ through point-by-point calculations.

3h–j) mirrored by a decrease of $\delta^{30}Si_{Si(OH)4}$ (Fig. 3m–o). This indicates biological consumption of $Si(OH)_4$ and fractionation of Si isotopes in the surface waters on the East China Sea mid-shelf and slope, while the lower $\delta^{30}Si_{Si(OH)4}$ signatures at depth (as well as at station PN08) were primarily controlled by BSi remineralization combined with admixture of the weakly fractionated deep waters. Note that surface salinity values at these stations varied between 33.0 and 34.0 (Fig. 3c–e) ruling out nutrient inputs via horizontal mixing of either the Changjiang Diluted Water or the Kuroshio Branch Current. The primary $Si(OH)_4$ source was thus vertical mixing from underlying waters.

The T-S distribution patterns displayed a similar linear relationship for the entire water column at stations PN06 and PN04 and for waters above the subsurface salinity maximum layer at station DH13 (Fig. 2a). Consequently, the initial condition for diatom growth in the surface waters at the three stations is the $\delta^{30}Si_{Si(OH)4}$ and $Si(OH)_4$ concentrations observed near the subsurface salinity maximum layer (i.e., +1.9‰ and 6.6 μmol L^{-1} of the sample from 125 m depth at station DH13; Tables 1 and 2), which show only minor seasonality and represent the nutrient inputs from the Kuroshio subsurface water into the East China Sea. Note that the depth of this source water is not spatially homogenous. Previous studies showed that the depth of the Kuroshio subsurface water upwelled onto the East China Sea shelf can vary between 100 and 300 m (Yang et al. 2011, 2012), which may further experience physical (e.g., mixing with other water masses) or biological (e.g., dissolution of sinking diatom frustules) alterations in the East China Sea. However, $\delta^{30}Si_{Si(OH)4}$ signatures were within the analytical error constant between 100 and 600 m at station DH13 (Fig. 3o; Table 1), as well as in the subsurface waters from comparable depths in the South China Sea (Cao et al. 2012) and from the subtropical gyre in the western North Pacific (Reynolds et al. 2006). In addition, isotopic effects of BSi dissolution would not be measurable in waters below 100 m in that the amount of regenerated Si would be too small to influence the isotopic composition of the large dissolved $Si(OH)_4$ reservoir.

Nevertheless, the analytical errors for $\delta^{30}Si_{Si(OH)4}$ and $Si(OH)_4$ concentration determinations in this study, which were ±0.25‰ and ±3%, respectively, were included to account for the possible variability of the initial condition defined by a single sample.

Using these initial values, the estimated average $^{30}\varepsilon_{upt}$ through point-by-point calculations was -0.7 ± 0.2‰ following the Rayleigh model (Eq. 3) and -1.3 ± 0.3‰ following the steady state model (Eq. 5) with *f* values of 0.2-0.3 (Eq. 2; Table 2). While the two $^{30}\varepsilon_{upt}$ values span the average of −1.1‰ from culture experiments (De La Rocha et al. 1997; Sutton et al., 2013), both values were within error consistent with those obtained on the inner shelf influenced by the Changjiang Diluted Water suggesting a constant in situ $^{30}\varepsilon_{upt}$ independent of source water properties in the East China Sea surface layer in summer. Note that our $^{30}\varepsilon_{upt}$ values following the steady state model are indistinguishable from the average of -1.2 ± 0.3‰ estimated from field investigations in both the Southern Ocean (Fripiat et al. 2011, and references therein) and the Pacific Ocean (e.g., Reynolds et al. 2006; Beucher et al. 2008). The narrow range of estimations for in situ $^{30}\varepsilon_{upt}$ indicates that mixed diatom assemblages in a natural system may have reduced the species-dependent variability (Fripiat et al. 2014), which was also observed for N isotope fractionation during NO_3 utilization (Sigman et al. 2009).

Dynamics of dissolved Si isotopes in the East China Sea in winter

Vertical mixing control of $\delta^{30}Si_{Si(OH)4}$ on the shelf

The China Coastal Current sourced from the west coast of the Korean Peninsula and driven by the northeast monsoon is a major water mass broadly following the Chinese coast in winter (Lee and Chao 2003). It generally has a salinity of below 33.0 and high $Si(OH)_4$ concentrations above 35.0 μmol L^{-1} at the mouth of the Changjiang estuary (Han et al. 2013). However, the winter surface salinity at the innermost station PN10 was >33.7 (Fig. 3a) and $Si(OH)_4$ concentrations were <10.0 μmol L^{-1} (Fig. 3f) indicating no obvious influence of the China Coastal Current during the sampling period. On the other hand, the surface salinity was below 34.0, suggesting minor contributions from the Kuroshio Branch Current to the nearshore East China Sea. In this context, the homogeneous property distributions at station PN10 in winter were most likely induced by the thorough mixing between preformed fractionated surface waters and deep waters with low $\delta^{30}Si_{Si(OH)4}$.

Both PT and salinity values increased gradually from station PN10 to station PN03b (Fig. 2b), indicating horizontal admixture of warm and saline waters onshore. However, the winter surface $\delta^{30}Si_{Si(OH)4}$ at the two endpoint stations of the transect were higher than those of the stations in between (Fig. 3k–o; Table 1), which would rule out horizontal mixing. BSi dissolution will lower the $\delta^{30}Si_{Si(OH)4}$ signatures, while any fractionation occurring during this process can currently not be quantified (Demarest et al. 2009; Sun et al. 2014; Wetzel et al. 2014) and remains to be validated in natural systems. As a consequence, vertical mixing primarily homogenized the property distributions on the East China Sea shelf, in particular in winter when the strong northeast monsoon and surface cooling substantially increases the vertical mixing with the deep waters (Chao 1991; Chen et al. 1994).

The vertical profiles of $\delta^{30}Si_{Si(OH)4}$ displayed no spatial variations among stations PN08, PN06, and PN04 (Fig. 3l–n) suggesting that the water column there was occupied by a uniform water mass, i.e., upwelled Kuroshio subsurface water. Values observed around the subsurface salinity maximum layer at station PN03b (i.e., +1.5‰ and 7.3 μmol L^{-1} of the sample from 150 m depth; Tables 1 and 2) were selected as the initial condition. All $\delta^{30}Si_{Si(OH)4}$ data collected in winter at the three stations were, however, essentially indistinguishable from the initial value with high *f* values of 0.8-1.0 (Eq. 2; Table 2). The negligible biological utilization would result in large uncertainties when estimating $^{30}\varepsilon_{upt}$ through point-by-point calculations. As a consequence, we infer that the relatively low $\delta^{30}Si_{Si(OH)4}$ signatures observed on the East China Sea shelf in winter were primarily a consequence of the admixture of the Kuroshio subsurface water without significant alterations originating from the biological fractionation of Si isotopes.

Horizontal admixture of the Kuroshio surface water near the shelf break

The surface salinity of >34.6 was higher than in subsurface waters at station PN03b in winter (Fig. 3e), suggesting that the extremely saline waters originated from intrusions at the surface rather than from the deeper layer of the Kuroshio Branch Current. Moreover, these surface waters were highly depleted in $Si(OH)_4$ (~1.0 μmol L^{-1}; Fig. 3j) reaching $\delta^{30}Si_{Si(OH)4}$ values close to +2.8‰ (Fig. 3o; Table 1), which agrees well with data obtained from the surface layer of the subtropical gyre in the western North Pacific (Reynolds et al. 2006). Horizontal admixture of the highly fractionated Kuroshio surface water was therefore limited to offshore areas beyond the East China Sea shelf break during the sampling period.

As shown in the $\delta^{30}Si_{Si(OH)4}$−1/$Si(OH)_4$ plot (Fig. 5), the data points are separated into two distinct clusters for the entire water column at stations PN08, PN06, and PN04 and in the surface waters at station PN03b in winter. Although they were all affected by the enhanced intrusion of the Kuroshio Branch Current, the Kuroshio surface water dominated the surface layer of the outermost station PN03b while other water bodies were largely influenced by the Kuroshio subsurface water. Moreover, the data show that no interactions occurred between the two major water masses since no data

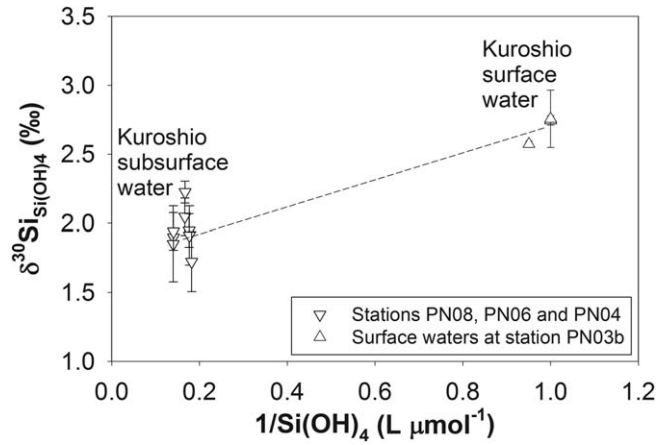

Fig. 5. $\delta^{30}Si_{Si(OH)4}$ vs. $1/Si(OH)_4$ for samples collected throughout the water column at stations PN08, PN06, and PN04 and in the surface waters at station PN03b in winter 2009. The dashed line indicates the schematic mixing curve between the two major water masses.

points were located on the mixing curve defined by the two end-members (Fig. 5).

Seasonal variability of dissolved Si isotopes on the East China Sea shelf

Minor seasonal differences in $\delta^{30}Si_{Si(OH)4}$ were observed in the surface waters at the innermost station PN10, where the summer bottom value was significantly lower than in winter (Fig. 3k). The dominant Changjiang Diluted Water in the nearshore surface waters was less fractionated in summer primarily owing to the relatively low degree of $Si(OH)_4$ utilization caused by the continuous supply of Si from the Changjiang discharge, which resulted in Si isotopic compositions comparable to those in the winter surface waters influenced by admixture of deep waters with low $\delta^{30}Si_{Si(OH)4}$. While the bottom $\delta^{30}Si_{Si(OH)4}$ in winter was increased via admixture of highly fractionated surface waters, the lower summer signature may have been induced by processes generating light Si isotope signals in the complex estuarine environment, such as dissolution of BSi or lithogenic silica introduced by the Changjiang.

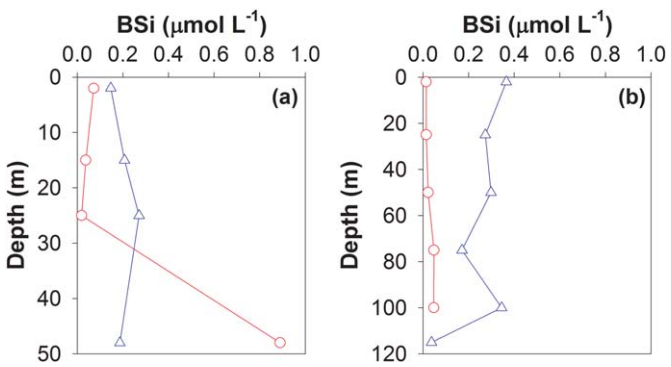

Fig. 6. Vertical distribution of biogenic silica (BSi) in suspended particles at stations (a) PN08 and (b) PN04 in summer (red circles and lines) and winter (blue triangles and lines) 2009. [Color figure can be viewed in the online issue, which is available at wileyonlinelibrary.com.]

In contrast, surface $\delta^{30}Si_{Si(OH)4}$ signatures at stations PN08, PN06, and PN04 on the East China Sea shelf were significantly higher in summer than in winter, whereas essentially uniform values were observed between seasons in the near-bottom waters (Fig. 3l–n). Given that $Si(OH)_4$ in these surface waters was primarily sourced from the Kuroshio subsurface water (excluding station PN08 influenced by the Changjiang Diluted Water in summer), this pattern most likely originated from the higher $Si(OH)_4$ consumption in the surface waters during summer than during winter as reflected by the contrasting f values (0.2-0.3 vs. 0.8-1.0; Table 2). This finding is consistent with the generally higher PP on the East China Sea shelf in summer than in winter (Gong et al. 2003; Liu et al. 2010) and diatoms dominating the phytoplankton community throughout the year (Guo et al. 2014).

Note that BSi in suspended particles collected at stations PN08 and PN04 displayed an apparently unexpected distribution with significantly lower concentrations in summer than in winter except in the near-bottom waters (Fig. 6). This pattern, in accordance with the distributions of fucoxanthin (a typical diatom pigment; data not shown), indicates higher standing stock of diatoms in the winter water column with, however, lower biological consumption. The apparent discrepancy between a near complete depletion of $Si(OH)_4$ not matched by an equivalent increase in BSi observed in this study, as well as in previous ones (e.g., Brzezinski et al. 2003; Leblanc et al. 2003; Cao et al. 2012) demonstrates that considerable BSi production had occurred but the majority of it had already been removed from the water column by additional processes such as particle settling and grazing, which lowered the BSi concentrations on the East China Sea shelf in summer (overall <0.1 μmol L^{-1} except in the near-bottom waters at station PN08; Table 3). In support of this, Chen et al. (2012) estimated that increasing temperature largely enhances phytoplankton losses to microzooplankton herbivory in eutrophic waters. On the other hand, the $Si(OH)_4$ decrease indicates net BSi production (i.e., gross production subtracted by dissolution) over a relatively long period of time, which will be integrated in the $\delta^{30}Si_{Si(OH)4}$ signatures reflecting biological alteration on timescales comparable to physical mixing. Information on suspended particles obtained from shipboard bottle BSi data can, however, only reflect a "snapshot" view and is frequently decoupled from the corresponding dissolved signatures (van Beek et al. 2007).

The East China Sea and the South China Sea are two major marginal sea systems of the western North Pacific, which are connected by water mass exchange through the Taiwan Strait (Han et al. 2013) and offshore through the Kuroshio Current (Chen 2008). While the South China Sea is characterized by an oligotrophic and permanently stratified

Table 3. Biogenic silica (BSi) concentration data collected at stations PN08 and PN04 during summer and winter cruises to the East China Sea in August 2009 and December 2009–January 2010.

		BSi (μmol L^{-1})	
Station	Depth (m)	Summer	Winter
PN08	2	0.07	0.15
	15	0.04	0.21
	25	0.02	0.27
	48	0.89	0.19
PN04	2	0.01	0.37
	25	0.01	0.27
	50	0.02	0.30
	75	0.05	0.17
	100	0.05	0.34
	115		0.04

deep basin, the East China Sea is dominated by a broad and relatively eutrophic shelf. Noteworthy is the lack of $\delta^{30}Si_{Si(OH)4}$ seasonality in the surface waters of the South China Sea (Cao et al. 2012), which is distinct on the East China Sea shelf. This is consistent with the seasonal pattern of PP, which displays no significant differences between summer and winter in both shelf and basin areas of the South China Sea (Ning et al. 2004; Chen and Chen 2006) while summer PP is generally higher than in winter on the East China Sea shelf (Gong et al. 2003; Liu et al. 2010). As determined by different trophic levels, diatoms play a more important role in the phytoplankton community on the East China Sea shelf (Guo et al. 2014) than in the South China Sea, where the picophytoplankton is overall more abundant (Ning et al. 2004). Consequently, diatoms in the East China Sea are sensitive to the significantly changing physical and/or chemical conditions resulting in the strong seasonality of dissolved Si isotopes (Fig. 3l–n).

On the other hand, $\delta^{30}Si_{Si(OH)4}$ signatures in the South China Sea show a larger range of variations (+1.0 to +3.0‰; Cao et al. 2012) than in the East China Sea (+1.5 to +3.0‰; Fig. 3k–o; Table 1), owing to the light isotopic composition of seawater below 1000 m in the South China Sea basin originating from the deep Pacific Ocean (Grasse et al. 2013). The highest surface $\delta^{30}Si_{Si(OH)4}$ is, however, identical between the two seas since both systems are influenced overall by the Kuroshio Current and the degree of Si isotope fractionation is largely constrained by almost the same initial conditions.

Implications

In summary, the seawater $\delta^{30}Si_{Si(OH)4}$ distribution in the East China Sea displayed distinct spatial and seasonal variations in summer 2009 and the subsequent winter, which were overall controlled by variable interaction between changes in water mass mixing and in biological utilization. As a result of the seasonally changing processes controlling $\delta^{30}Si_{Si(OH)4}$ dynamics, the majority of summer surface values obtained on the East China Sea shelf were higher than those in winter, suggesting an overall higher Si utilization resulting from enhanced diatom productivity in summer compared with winter.

Significant nutrient inputs from Changjiang were only detected on the inner shelf in summer, whereas the primary $Si(OH)_4$ source of the surface waters of the East China Sea was advective supply by the Kuroshio subsurface water. Thus, despite the size of the Changjiang, nutrient supply from the open ocean was more important than riverine nutrient inputs in the East China Sea during the sampling period, which may have implications for other marginal seas. Note that construction of dams increases on a global scale and river damming can decrease $Si(OH)_4$ concentrations and increase $\delta^{30}Si_{Si(OH)4}$ signatures downstream (Hughes et al. 2012). However, this may have only been relevant near the river mouth where the isotopic composition of continental Si supply to the ocean and the estuarine phytoplankton community and ecosystem are impacted. Further work is required to better understand the anthropogenic effects on Si biogeochemical cycling in marginal seas, in particular in river-coast ecosystems.

While minor biological consumption in winter prevents a reliable evaluation of the Si isotope fractionation during diatom growth in the East China Sea, the estimated $^{30}\varepsilon_{upt}$ values based on the summer data set are generally comparable to those obtained from culture experiments (De La Rocha et al. 1997; Sutton et al. 2013). However, the apparent $^{30}\varepsilon_{upt}$ obtained in this study represents a fractionation factor of naturally mixed diatom assemblages, which integrated the effect of both BSi production and dissolution, and even the mixing between Si pools differently fractionated by different species. Nevertheless, our $^{30}\varepsilon_{upt}$ values following the steady state model agree well with the average of -1.2 ± 0.3‰ estimated from field investigations in the open ocean (Fripiat et al. 2014). Given the contrasting physicobiogeochemical conditions between the East China Sea and for instance the Southern Ocean, this consistence points to a constant in situ $^{30}\varepsilon_{upt}$ in the world's oceans.

References

Beucher, C. P., M. A. Brzezinski, and J. L. Jones. 2008. Sources and biological fractionation of silicon isotopes in the Eastern Equatorial Pacific. Geochim. Cosmochim. Acta **72**: 3063–3073. doi:10.1016/j.gca.2008.04.021

Brzezinski, M. A., J. L. Jones, K. D. Bidle, and F. Azam. 2003. The balance between silica production and silica dissolution in the sea: Insights from Monterey Bay, California, applied to the global data set. Limnol. Oceanogr. **48**: 1846–1854. doi:10.4319/lo.2003.48.5.1846

Cao, Z., M. Frank, M. Dai, P. Grasse, and C. Ehlert. 2012. Silicon isotope constraints on sources and utilization of silicic acid in the northern South China Sea. Geochim. Cosmochim. Acta **97**: 88–104. doi:10.1016/j.gca.2012.08.039

Cardinal, D., L. Y. Alleman, F. Dehairs, N. Savoye, T. W. Trull, and L. Andre. 2005. Relevance of silicon isotopes to Si-nutrient utilization and Si-source assessment in Antarctic waters. Global Biogeochem. Cycles **19**. doi:10.1029/2004GB002364

Chao, S.-Y. 1991. Circulation of the East China Sea, A numerical study. J. Oceanogr. Soc. Japan **46**: 273–295. doi:10.1007/BF02123503

Chen, B., M. R. Landry, B. Huang, and H. Liu. 2012. Does warming enhance the effect of microzooplankton grazing on marine phytoplankton in the ocean? Limnol. Oceanogr. **57**: 519–526. doi:10.4319/lo.2012.57.2.0519

Chen, C., R. C. Beardsley, R. Limeburner, and K. Kim. 1994. Comparison of winter and summer hydrographic observations in the Yellow and East China Seas and adjacent Kuroshio during 1986. Cont. Shelf Res. **14**: 909–929. doi:10.1016/0278-4343(94)90079-5

Chen, C., and others. 2008. Physical mechanisms for the offshore detachment of the Changjiang Diluted Water in the East China Sea. J. Geophys. Res. **113**: C02002. doi:10.1029/2006JC003994

Chen, C.-T. A. 1996. The Kuroshio intermediate water is the major source of nutrients on the East China Sea continental shelf. Oceanol. Acta **19**: 523–527.

Chen, C.-T. A. 2008. Distributions of nutrients in the East China Sea and the South China Sea Connection. J. Oceanogr. **64**: 737–751. doi:10.1007/s10872-008-0062-9

Chen, C.-T. A., R. Ruo, S.-C. Pai, C.-T. Liu, and G. T. F. Wong. 1995. Exchange of water masses between the East China Sea and the Kuroshio off northeastern Taiwan. Cont. Shelf Res. **15**: 19–39. doi:10.1016/0278-4343(93)E0001-O

Chen Y.-L. L., and H.-Y. Chen. 2006. Seasonal dynamics of primary and new production in the northern South China Sea: The significance of river discharge and nutrient advection. Deep-Sea Res. I **53**: 971–986. doi:10.1016/j.dsr.2006.02.005

Chern C.-S., J. Wang, and D.-P. Wang. 1990. The exchange of Kuroshio and East China Sea shelf water. J. Geophys. Res. **95**: 16017–16023. doi:10.1029/JC095iC09p16017

Chiang, K.-P., Y.-T. Chen, and G.-C. Gong. 1999. Spring distribution of diatom assemblages in the East China Sea. Mar. Ecol. Prog. Ser. **186**: 75–86. doi:10.3354/meps186075

Chiang, K.-P., Y.-H. Chou, J. Chang, and G.-C. Gong. 2004. Winter distribution of diatom assemblages in the East China Sea. J. Oceanogr. **60**: 1053–1062. doi:10.1007/s10872-005-0013-7

De La Rocha, C. L., M. A. Brzezinski, and M. J. DeNiro. 1997. Fractionation of silicon isotopes during biogenic silica formation. Geochim. Cosmochim. Acta **61**: 5051–5056. doi:10.1016/S0016-7037(97)00300-1

Demarest, M. S., M. A. Brzezinski, and C. P. Beucher. 2009. Fractionation of silicon isotopes during biogenic silica dissolution. Geochim. Cosmochim. Acta **73**: 5572–5583. doi:10.1016/j.gca.2009.06.019

de Souza, G. F., B. C. Reynolds, J. Rickli, M. Frank, M. A. Saito, L. J. A. Gerringa, and B. Bourdon. 2012. Southern Ocean control of silicon stable isotope distribution in the deep Atlantic Ocean. Global Biogeochem. Cycles **26**: GB2035. doi:10.1029/2011GB004141

Du, C., and others. 2013. Impact of the Kuroshio intrusion on the nutrient inventory in the upper northern South China Sea: Insights from an isopycnal mixing model. Biogeosciences **10**: 6419–6432. doi:10.5194/bg-10-6419-2013

Ehlert, C., and others. 2012. Factors controlling the silicon isotope distribution in waters and surface sediments of the Peruvian coastal upwelling. Geochim. Cosmochim. Acta **99**: 128–145. doi:10.1016/j.gca.2012.09.038

Fripiat, F., A.-J. Cavagna, N. Savoye, F. Dehairs, L. André, and D. Cardinal. 2011. Isotopic constraints on the Si-biogeochemical cycle of the Antarctic Zone in the Kerguelen area (KEOPS). Mar. Chem. **123**: 11–22. doi:10.1016/j.marchem.2010.08.005

Fripiat, F., J.-L. Tison, L. André, D. Notz, and B. Delille. 2014. Biogenic silica recycling in sea ice inferred from Si-isotopes: Constraints from Arctic winter first-year sea ice. Biogeochemistry **119**: 25–33. doi:10.1007/s10533-013-9911-8

Furuya, K., M. Hayashi, Y. Yabushita, and A. Ishikawa. 2003. Phytoplankton dynamics in the East China Sea in spring and summer as revealed by HPLC-derived pigment signatures. Deep-Sea Res. II **50**: 367–387. doi:10.1016/S0967-0645(02)00460-5

Furuya, K., K. Kurita, and T. Odate. 1996. Distribution of phytoplankton in the East China Sea in the winter of 1993. J. Oceanogr. **52**: 323–333. doi:10.1007/BF02235927

Gaston, T. F., T. A. Schlacher, and R. M. Connolly. 2006. Flood discharges of a small river into open coastal waters: Plume traits and material fate. Estuarine Coastal Shelf Sci. **69**: 4–9. doi:10.1016/j.ecss.2006.03.015

Georg, R. B., B. C. Reynolds, M. Frank, and A. N. Halliday. 2006. New sample preparation techniques for the determination of Si isotopic compositions using MC-ICPMS. Chem. Geol. **235**: 95–104. doi:10.1016/j.chemgeo.2006.06.006

Gong, G.-C., J. Chang, K.-P. Chiang, T.-M. Hsiung, C.-C. Hung, S.-W. Duan, and L. A. Codispoti. 2006. Reduction of primary production and changing of nutrient ratio in the East China Sea: Effect of the Three Gorges Dam? Geophys. Res. Lett. **33**: L07610, doi:10.1029/2006GL025800

Gong, G.-C., Y.-H. Wen, B.-W. Wang, and G.-J. Liu. 2003. Seasonal variation of chlorophyll *a* concentration, primary production and environmental conditions in the

subtropical East China Sea. Deep-Sea Res. II **50**: 1219–1236. doi: 10.1016/S0967-0645(03)00019-5

Grasse, P., C. Ehlert, and M. Frank. 2013. The influence of water mass mixing on the dissolved Si isotope composition in the Eastern Equatorial Pacific. Earth Planet. Sci. Lett. **380**: 60–71. doi:10.1016/j.epsl.2013.07.033

Guo, S., Y. Feng, L. Wang, M. Dai, Z. Liu, Y. Bai, and J. Sun. 2014. Seasonal variation in the phytoplankton community of a continental-shelf sea: The East China Sea. Mar. Ecol. Prog. Ser. **516**: 103–126. doi:10.3354/meps10952

Han, A., and others. 2013. Inter-shelf nutrient transport from the East China Sea as a major nutrient source supporting winter primary production on the northeast South China Sea shelf. Biogeosciences **10**: 8159–8170. doi:10.5194/bg-10-8159-2013

Hughes, H. J., S. Bouillon, L. André, and D. Cardinal. 2012. The effects of weathering variability and anthropogenic pressures upon silicon cycling in an intertropical watershed (Tana River, Kenya). Chem. Geol. **308-309**: 18–25. doi:10.1016/j.chemgeo.2012.03.016

Ichikawa, H., and R. C. Beardsley. 2002. The current system in the Yellow and East China Seas. J. Oceanogr. **58**: 77–92. doi:10.1023/A:1015876701363

Karl, D. M., and G. Tien. 1992. MAGIC: A sensitive and precise method for measuring dissolved phosphorus in aquatic environments. Limnol. Oceanogr. **37**: 105–116. doi:10.4319/lo.1992.37.1.0105

Leblanc, K., B. Quéguiner, N. Garcia, P. Rimmelin, and P. Raimbault. 2003. Silicon cycle in the NW Mediterranean Sea: Seasonal study of a coastal oligotrophic site. Oceanol. Acta **26**: 339–355. doi:10.1016/S0399-1784(03)00035-5

Lee, H.-J., and S.-Y. Chao. 2003. A climatological description of circulation in and around the East China Sea. Deep-Sea Res. II **50**: 1065–1084. doi:10.1016/S0967-0645(03)00010-9

Li, M., K. Xu, M. Watanabe, and Z. Chen. 2007. Long-term variations in dissolved silicate, nitrogen, and phosphorus flux from the Yangtze River into the East China Sea and impacts on estuarine ecosystem. Estuarine Coastal Shelf Sci. **71**: 3–12. doi:10.1016/j.ecss.2006.08.013

Lie, H.-J., C.-H. Cho, J.-H. Lee, and S. Lee. 2003. Structure and eastward extension of the Changjiang River plume in the East China Sea. J. Geophys. Res. **108**: 3077. doi: 10.1029/2001JC001194

Liu, K.-K., S.-Y. Chao, H.-J. Lee, G.-C. Gong, and Y.-C. Teng. 2010. Seasonal variation of primary productivity in the East China Sea: A numerical study based on coupled physical-biogeochemical model. Deep-Sea Res. II **57**: 1762–1782. doi:10.1016/j.dsr2.2010.04.003

Liu, K.-K., T.-H. Peng, P.-T. Shaw, and F.-K. Shiah. 2003. Circulation and biogeochemical processes in the East China Sea and the vicinity of Taiwan: An overview and a brief synthesis. Deep-Sea Res. II **50**: 1055–1064. doi:10.1016/S0967-0645(03)00009-2

Liu, Y., M. Dai, W. Chen, and Z. Cao. 2011. Distribution of biogenic silica in the upwelling zones in the South China Sea, p. 55–65. In C.-C. Wu and J. Gan, [eds.], Advances in geosciences: Atmospheric science and ocean science, vol **28**. World Scientific Publishing Company.

Ning, X., F. Chai, H. Xue, Y. Cai, C. Liu, and J. Shi. 2004. Physical-biological oceanographic coupling influencing phytoplankton and primary production in the South China Sea. J. Geophys. Res. **109**: C10005. doi:10.1029/2004JC002365

Ragueneau, O., N. Savoye, Y. Del Amo, J. Cotton, B. Tardiveau, and A. Leynaert. 2005. A new method for the measurement of biogenic silica in suspended matter of coastal waters: using Si:Al ratios to correct for the mineral interference. Cont. Shelf Res. **25**: 697–710. doi:10.1016/j.csr.2004.09.017

Reynolds, B. C., and others. 2007. An inter-laboratory comparison of Si isotope reference materials. J. Anal. Atomic Spectrom. **22**: 561–568. doi:10.1039/b616755a

Reynolds, B. C., M. Frank, and A. N. Halliday. 2006. Silicon isotope fractionation during nutrient utilization in the North Pacific. Earth Planet. Sci. Lett. **244**. doi:10.1016/j.epsl.2006.02.002

Schlitzer, R. 2015. Ocean Data View 4. Available from http://odv.awi.de.

Sigman, D. M., K. L. Karsh, and K. L. Casciotti. 2009. Ocean process tracers: Nitrogen isotopes in the ocean, p. 4138–4153. In J. H. Steele, S. A. Thorpe, and K. K. Turekian [eds.], Encyclopedia of ocean sciences, 2nd ed. Academic Press, London.

Suga, T., A. Kato, and K. Hanawa. 2000. North Pacific Tropical Water: Its climatology and temporal changes associated with the climate regime shift in the 1970s. Prog. Oceanogr. **47**: 223–256. doi:10.1016/S0079-6611(00)00037-9

Sun, X., M. Olofsson, P. S. Andersson, B. Fry, C. Legrand, C. Humborg, and C.-M. Mörth. 2014. Effects of growth and dissolution on the fractionation of silicon isotopes by estuarine diatoms. Geochim. Cosmochim. Acta **130**: 156–166. doi:10.1016/j.gca.2014.01.024

Sutton, J. N., D. E. Varela, M. A. Brzezinski, and C. P. Beucher. 2013. Species-dependent silicon isotope fractionation by marine diatoms. Geochim. Cosmochim. Acta **104**: 300–309. doi:10.1016/j.gca.2012.10.057

van Beek, P., R. François, M. Conte, J.-L. Reyss, M. Souhaut, and M. Charette. 2007. $^{228}Ra/^{226}Ra$ and $^{226}Ra/Ba$ ratios to track barite formation and transport in the water column. Geochim. Cosmochim. Acta **71**: 71–86. doi:10.1016/j.gca.2006.07.041

Wang, G., M. Dai, S. S. P. Shen, Y. Bai, and Y. Xu. 2014. Quantifying uncertainty sources in the gridded data of sea surface CO_2 partial pressure. J. Geophys. Res. Oceans **119**: 5181–5189. doi:10.1002/2013JC009577

Wetzel, F., G. F. de Souza, and B. C. Reynolds. 2014. What controls silicon isotope fractionation during dissolution of diatom opal? Geochim. Cosmochim. Acta **131**: 128–137. doi:10.1016/j.gca.2014.01.028

Wong, G. T. F., S.-Y. Chao, Y.-H. Li, and F.-K. Shiah. 2000. The Kuroshio edge exchange process (KEEP) study-an introduction to hypotheses and highlights. Cont. Shelf Res. **20**: 335–347. doi:10.1016/S0278-4343(99)00075-8

Yang, D., B. Yin, Z. Liu, T. Bai, J. Qi, and H. Chen. 2012. Numerical study on the pattern and origins of Kuroshio branches in the bottom water of southern East China Sea in summer. J. Geophys. Res. **117**: C02014. doi:10.1029/2011JC007528

Yang, D., B. Yin, Z. Liu, and X. Feng. 2011. Numerical study of the ocean circulation on the East China Sea shelf and a Kuroshio bottom branch northeast of Taiwan in summer. J. Geophys. Res. **116**: C05015. doi:10.1029/2010JC006777

Acknowledgments

We would like to thank Danna Wang, Tao Huang, Chuanjun Du, Feifei Meng, and Kai Wu for help with the ancillary data collection and the crew of R/V *Dongfanghong II* for their assistance in sample collection. We thank Jianyu Hu for providing the CTD data and Lei Wang and Bangqin Huang for providing the fucoxanthin data. John Hodgkiss is thanked for his assistance in polishing the manuscript's English. Comments from the editors and two anonymous reviewers have significantly improved the quality of this contribution.

This work was funded by the National Key Scientific Research Project (2015CB954000) and the National Basic Research Program (973) (2009CB421200) sponsored by the Ministry of Science and Technology of the PRC. This work was also funded by the National Natural Science Foundation of China through grants 91328202, 41121091, 90711005, and 41130857. Zhimian Cao was supported by a Research Fellowship for postdoctoral researchers by the Alexander von Humboldt Foundation.

Submitted 30 December 2014
Revised 30 April 2015
Accepted 18 May 2015

Associate editor: Maren Voss